

Highlights

- Efficiency of topology optimization algorithm for metamaterials design are improved by coupling with reduced order models.
- Isogeometric analysis based on Bézier extraction provide solutions with smoother manifold for constructing the reduced basis.
- Sensitivity calculation methods including the residual error are derived in the level set method.

Three-dimensional topology optimization of auxetic metamaterial using isogeometric analysis and model order reduction

Chuong Nguyen^a, Xiaoying Zhuang^{a,1,*}, Ludovic Chamoin^{b,2,*}, Hung Nguyen-Xuan^c, Xianzhong Zhao^d, Timon Rabczuk^{e,3,*}

^a*Institute of Continuum Mechanics, Leibniz Universität Hannover, Hannover, Germany*

^b*LMT, ENS Paris-Saclay, CNRS, Université Paris-Saclay 61 Avenue du Président Wilson, 94235 Cachan, France*

^c*CIRTECH Institute, Ho Chi Minh City University of Technology (HUTECH), Ho Chi Minh City, Vietnam*

^d*College of Civil Engineering, Tongji University, China*

^e*Institute of Structural Mechanics, Bauhaus-Universität Weimar, Weimar, Germany*

Abstract

In this work, we present an efficiently computational approach for designing material micro-structures by means of topology optimization. The central idea relies on using the isogeometric analysis integrated with the parameterized level set function for numerical homogenization, sensitivity calculation and optimization of the effective elastic properties. Design variables, which are level set values associated with control points, are updated from the optimizer and represent the geometry of the unit cell. We further improve the computational efficiency in each iteration by employing reduced order modeling when solving linear systems of the equilibrium equations. We construct a reduced basis by reusing computed solutions from previous optimization steps, and a much smaller linear system of equations is solved on the reduced basis. Two- and three-dimensional numerical results show the effectiveness of the topology optimization algorithm coupled with the reduced basis approach in designing metamaterials.

Keywords: metamaterials, topology optimization, reduced order model, isogeometric analysis, Bézier extraction

1. Introduction

Metamaterials are classified as artificial composites possessing extraordinary mechanical behaviors that are not available in nature. They have received attention in scientific applications and engineering over the last decades. Typically the class of auxetic metamaterials having properties of negative Poisson's ratio (NPR) have shown potential applications from biomedical to defense problems [1, 2]. Modifying the effective Poisson's ratio, which affects kinematic deformations, can enhance the performance of embedded structures. The material functionalities are attained by rationally designing their microstructure layouts. Among material design methods, shape and topology optimization for primitive cells has been considered as a prominent method for materials functionality design.

Topology optimization generally involves iterative searching for material distribution within design domains. In the density-based topology optimization, the void and solid regions of material

*Corresponding authors

¹zhuang@ikm.uni-hannover.de

²ludovic.chamoin@ens-paris-saclay.fr

³timon.rabczuk@uni-weimar.de

are represented by density values, which are also considered as design variables. Among the density approaches, the evolutionary structural optimization (ESO) [3, 4] and solid isotropic material with penalization (SIMP) method [5] are frequently used in structural and material optimization [6, 7] due to the efficiency and easy implementation. Alternatively, the level set method represents structural boundaries by a zero level set function, which enables flexible changes in shape and topology with distinct material interfaces. Various optimization problems have been successfully implemented with the level set approach, e.g., structure compliance minimization [8, 9], frequency response problem [10], or design of metamaterials with negative Poisson’s ratio [11, 12].

In microstructure topology optimization, the effective properties of unit cells are determined by a numerical homogenization procedure. This involves solving linear systems of equilibrium equations and requires high computational cost. In order to circumvent this issue, reduced order modeling using Krylov subspaces [13, 14] has been proposed to enhance the efficiency. Large linear systems are solved by an iterative solver and using a search space from the previous linear system. The approach assumes that numerical stiffness from two consecutive iterations are slightly different due to minor changes in shapes or topology of structures. Alternatively, the reduced-basis approaches approximate high-dimensional solutions by the projection of the original model into a lower-dimensional subspace which is spanned by global basis functions or truncated modes. This surrogate model was employed in nonlinear structural optimization [15], multiscale homogenization [16]. Similarly, Gogu [17] proposed a reduced basis constructed from displacements which are calculated from a set of similar configurations. The original linear system is then projected on the reduced basis with a smaller size. The method has shown much improvement in structural topology optimization.

The motivation for using isogeometric analysis [18, 19] so far is due to higher-order approximation with the B-Spline or NURBS basis functions which are compatible with CAD tools. It enables to model the geometry in computer-aided design exactly, and the basis functions used to represent the geometry can directly approximate solution fields in numerical computation. Recently, this framework has also been used in various optimization problems, i.e., [20] with level set functions, [21] using the SIMP approach in structural optimization and [22] for auxetic metamaterials. Several works in [23, 24] introduced IGA coupled with reduced order models (ROM) to alleviate the computational cost for parameterized geometry model, and have shown an improvement in both accuracy and efficiency compared to the finite element method. We also mention the shape optimization problems in which the geometry parameters assigned as design variables are efficiently optimized with the combination of reduced order approaches. For example in [25], the proper generalized decomposition (PGD) was introduced to compute in an offline phase the parametric solutions for selected parameters which involve the sensitivity information provided. A similar strategy for parameter optimization may be applied with the isogeometric framework, such as [26], where model reduction based on PGD provides parametric solutions with much lower computation cost.

In this work, we exploit advantages of the parameterized level set method using the isogeometric setting for metamaterials design. This approach possibly allows using basis functions with higher orders to approximate the displacement field and the level set function. We further integrate reduced order modeling to improve the efficiency of the topology optimization algorithm. The proper coupling of reduced order techniques in an isogeometric framework is attractive and feasible due to the fact that the reduced basis is constructed from a smoother manifold of the isogeometric solution, and the optimized geometry is subsequently generated from the reduced solutions with saving computational time. We provide sensitivity analysis involving the reduced solutions in the level set framework. Metamaterial structures are designed in two and three dimensions to show the efficiency and reliability of the approach.

The paper is organized as follows: in [Section 2](#), we briefly discuss numerical homogenization methods and formulation for the effective elasticity tensor. [Section 3](#) introduces the parameterized

version of the level set function. In [Section 4](#), the discretized formulation with the isogeometric analysis using Bézier extraction for the numerical analysis is given. Afterward, the construction of the reduced basis is reviewed in [Section 5](#), and in [Section 6](#) the sensitivity analysis involving reduced solutions of effective coefficients is described. Numerical examples are presented in [Section 7](#) and followed by the conclusion in [Section 8](#).

2. Homogenization method

Heterogeneity of composite materials by nature requires fine scale discretization to capture the geometric details; this leads to large finite element models and increased computational burden. An alternative material modeling is to replace heterogeneity with an effective homogeneous model by considering a representative volume that can describe the equivalent properties at the macroscopic scale. The classical approach is based on the assumption of periodic arrangement of the microstructures, and it also considers that the length scale of the periodic structures is small when compared to dimensions of the macroscopic structure. The study of macroscopic properties is conventionally replaced by considering of a single unit cell alone.

Several analytical approaches are available to evaluate the effective properties of composites. For example, considering the volume fraction of a single inclusion embedded into an infinite matrix material, the effective properties were derived by Eshelby [\[27\]](#). Further developments from this approach and widely employed in modeling homogenized material can be found in the work by Mori and Tanaka [\[28\]](#), or self-consistent scheme by Hill [\[29\]](#). These analysis methods mainly deal with simple geometries of inclusions, i.e., circles or ellipses. In the context of topology optimization, complex geometries of the unit cell frequently occur and the analytical models are not able to predict effective properties of composites.

Numerical approaches have been developed to address the problem. From macroscopic strains, stresses and strain energy density, the effective elasticity of inhomogeneous materials was derived using a direct average method [\[30–32\]](#). Similarly, Zhang et al. [\[33\]](#) used the strain energy-based methods to predict effective properties in microstructure topology optimization. The work of Guedes and Kikuchi [\[34\]](#), or Sanchez-Palencia [\[32\]](#) introduced a rigorous mathematical theory for deriving effective elasticity coefficients by using weak-form of equilibrium equation and limits theory, namely asymptotic homogenization method. Another mathematical derivation for homogenized elasticity which is based on the governing equations with strong formulation can be found in the work by Zhuang et al. [\[35\]](#), and a similar framework for multi-field problems was recently investigated by Fantoni et al. [\[36\]](#).

The design of metamaterials in this work relies on the asymptotic homogenization method. Effective properties across a unit cell are obtained from a homogenization procedure with assumptions of periodicity and scale separation over the unit cell with overall macroscopic dimensions. A brief explanation of the asymptotic homogenization method used in this paper is given in the following and details of derivation can be found in [\[34, 37\]](#).

Due to local changes of material properties, the displacement expression is dependent on the small parameter ϵ and written as an asymptotic expansion:

$$\mathbf{u}^\epsilon(\mathbf{x}, \mathbf{y}, \epsilon) = \mathbf{u}^0(\mathbf{x}) + \epsilon \mathbf{u}^1(\mathbf{x}, \mathbf{y}) + \epsilon^2 \mathbf{u}^2(\mathbf{x}, \mathbf{y}) + \dots \quad \text{with} \quad \mathbf{y} = \mathbf{x}/\epsilon, \quad (1)$$

\mathbf{x} and \mathbf{y} are macroscopic and microscopic (unit cell) coordinates respectively. The displacement \mathbf{u}^ϵ

of the composite body is solution to the variational problem

$$\int_{\Omega} \boldsymbol{\varepsilon}(\mathbf{u}^\epsilon) : \mathbb{C} : \boldsymbol{\varepsilon}(\mathbf{v}) \, d\Omega = \int_{\Omega} \mathbf{b} \cdot \mathbf{v} \, d\Omega + \int_{\Gamma} \tilde{\mathbf{t}} \cdot \mathbf{v} \, d\Gamma, \quad (2)$$

where \mathbf{v} is the test function and $\boldsymbol{\varepsilon}$ is the mechanical strain. Body forces \mathbf{b} and surface tractions $\tilde{\mathbf{t}}$ are assumed not to vary over the microscopic domain. In the following procedure only the first and second variation terms of the displacement expansion (1) are employed to derive the effective elasticity tensor, and due to the linearity of the problem the second term can be written as

$$\mathbf{u}^1(\mathbf{x}, \mathbf{y}) = \boldsymbol{\chi}(\mathbf{x}, \mathbf{y}) \boldsymbol{\varepsilon}(\mathbf{u}^0(\mathbf{x})), \quad (3)$$

where $\boldsymbol{\chi}(\mathbf{x}, \mathbf{y})$ is the characteristic displacement. By substituting the asymptotic expansion (1) into (2) and applying the asymptotic analysis of the periodic functions in a unit cell [34], the following equilibrium equation is obtained

$$\int_Y \varepsilon_{pq}(\boldsymbol{\chi}^{mn}) C_{pqrs}(\mathbf{y}) \varepsilon_{rs}(\mathbf{v}) \, dY = \int_Y \varepsilon_{pq}^{0,mn} C_{pqrs}(\mathbf{y}) \varepsilon_{rs}(\mathbf{v}) \, dY \quad \forall \mathbf{v} \in V_0 \subset H^1, \quad (4)$$

where $\varepsilon^{0,mn}$ is the unit strain. The superior index mn indicates the test cases. For a two-dimensional problem, there are three independent unit strains $\boldsymbol{\varepsilon}^{0,11} = [1, 0, 0]$, $\boldsymbol{\varepsilon}^{0,22} = [0, 1, 0]$ and $\boldsymbol{\varepsilon}^{0,12} = [0, 0, 1]$. The characteristic displacements $\boldsymbol{\chi}^{mn}$ are obtained numerically under periodic condition in the unit cell Y . Having these local solutions, the effective elasticity tensor \mathbb{C}^H of the unit cell is calculated by

$$C_{ijkl}^H = \frac{1}{|Y|} \int_Y (\varepsilon_{pq}^{0,ij} - \varepsilon_{pq}(\boldsymbol{\chi}^{ij})) C_{pqrs}(\mathbf{y}) (\varepsilon_{rs}^{0,kl} + \varepsilon_{rs}(\boldsymbol{\chi}^{kl})) \, d\Omega, \quad (5)$$

which essentially corresponds to the average of strain energy in the unit cell.

3. Level set function

In this section we briefly discuss the fundamentals of the level set method in structural optimization. The material distribution in the unit cell is represented via an implicit level set function defined in a reference domain Y as shown in Fig. 1(a) with

$$\begin{cases} \phi(\mathbf{x}) > 0, & \mathbf{x} \in \Omega \text{ (solid)} \\ \phi(\mathbf{x}) < 0, & \mathbf{x} \in Y/\Omega \text{ (void)} \\ \phi(\mathbf{x}) = 0, & \mathbf{x} \in \partial\Omega \text{ (boundary)}. \end{cases} \quad (6)$$

The interfaces between void and solid parts are considered as design boundaries. The evolution of the design boundaries in the optimization process are handled by dynamic moving of the zero level set $\phi(\mathbf{x}(\tau), \tau) = 0$. The dynamic change in time is governed by the Hamilton–Jacobi (H-J) equation

$$\frac{\partial \phi}{\partial t} - V_n |\nabla \phi| = 0, \quad V_n = \frac{d\mathbf{x}}{dt} \cdot \frac{\nabla \phi}{|\nabla \phi|}, \quad (7)$$

where V_n is the normal velocity component. In the steepest descend method, V_n is chosen such that the gradient of the objective function is negative to ensure the objective function is minimized.

Conventionally, the level set function is updated by solving the Hamilton–Jacobi equation with a finite difference scheme [38, 39], and consequently a new design boundary is obtained and used to proceed with a next optimization iteration. It is noted that a restriction of step sizes is necessary to ensure numerical stability when solving the H–J equation with finite difference schemes, i.e., Courant–Friedrichs–Lewy (CFL) condition. Furthermore, the signed distance characteristic of the level set function should be maintained during the optimization procedure to avoid the flatness or steepness; therefore, additional re-initialization steps are provided periodically after several iterations [39, 40].

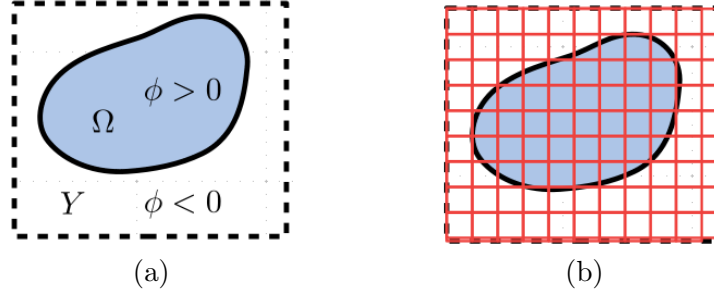


Figure 1: Unit cell geometry represented by a level set function (a) and fixed mesh on a square domain (b).

In this present work, the parameterized level set method (PLSM) [12, 41] is used. The level set function is approximated by

$$\phi(\mathbf{x}, \tau) = \sum_I^{ncp} R_I(\mathbf{x}) \alpha_I(\tau) = \mathbf{R}(\mathbf{x}) \cdot \boldsymbol{\alpha}(\tau), \quad (8)$$

and the H–J PDE equation reduces to an ordinary differential equation

$$\mathbf{R}^T \frac{d\boldsymbol{\alpha}}{d\tau} - V_n |(\nabla \mathbf{R})^T \boldsymbol{\alpha}| = 0 \quad \text{or} \quad V_n = \frac{\mathbf{R}^T \dot{\boldsymbol{\alpha}}}{|(\nabla \mathbf{R})^T \boldsymbol{\alpha}|} \quad (9)$$

where $R_I(\mathbf{x})$ are B-spline basis functions in the isogeometric concept. These functions will be discussed in Section 4. Herein, the expansion coefficients α_I are considered as design variables. The level set function is updated by changing values of the coefficients α_I during the optimization procedure. A gradient-based mathematical programming optimizer is used to optimize the design variables. Solving the H–J equation is avoided and the limit of step sizes to ensure numerical stability is unnecessary, so that the efficiency is improved. Furthermore, there is no re-initialization step to keep the level set function to be a signed distance function.

For a unit cell with two material phases, solid and void, as shown in Fig. 1(a), we can express spatial dependence in the elasticity tensor with a Heaviside function $\mathcal{H}(\phi)$ of the level set value. Equations (4) and (5) are written as

$$\int_Y \varepsilon_{pq}(\boldsymbol{\chi}^{ij}) C_{pqrs} \mathcal{H}(\phi(\mathbf{y})) \varepsilon_{rs}(\mathbf{v}) d\Omega = \int_Y \varepsilon_{pq}^{0,ij} C_{pqrs} \mathcal{H}(\phi(\mathbf{y})) \varepsilon_{rs}(\mathbf{v}) d\Omega, \quad (10)$$

$$C_{ijkl}^H = \frac{1}{|Y|} \int_Y (\varepsilon_{pq}^{0,ij} - \varepsilon_{pq}(\boldsymbol{\chi}^{ij})) C_{pqrs} \mathcal{H}(\phi(\mathbf{y})) (\varepsilon_{rs}^{0,kl} - \varepsilon_{rs}(\boldsymbol{\chi}^{kl})) d\Omega, \quad (11)$$

and for the volume of solid part

$$V = \int_Y \mathcal{H}(\phi(\mathbf{y})) d\Omega. \quad (12)$$

To obtain the derivative of the Heaviside function numerically, we use a regularized Heaviside function of the form

$$\mathcal{H}(\phi) = \begin{cases} \rho_{\min} & \phi < \xi \\ \frac{3}{4} \left(\frac{\phi}{\xi} - \frac{\phi^3}{3\xi^3} \right) + \frac{1}{2} & -\xi \leq \phi \leq \xi \\ 1 & \phi > \xi \end{cases} \quad (13)$$

where ξ is the smooth length, and $\rho_{\min} = 10^{-6}$ is chosen to avoid singularity in the numerical stiffness.

4. Isogeometric analysis with Bézier extraction

This section gives a brief description of the isogeometric analysis (IGA) concept [19] and the Bernstein-Bézier representation [42] to non-uniform rational basis functions (NURBS). Similar to the finite element approach, the actual geometry in the physical space is represented in a parameter space by using a mapping

$$\mathbf{T}(\boldsymbol{\xi}) = \sum_{I=1}^{ncp} R_I(\boldsymbol{\xi}) \mathbf{P}_I, \quad (14)$$

with a mesh of ncp control points \mathbf{P}_I and associated weight w_I . The NURBS basis functions $R_I(\boldsymbol{\xi})$ are defined as

$$R_I(\boldsymbol{\xi}) = \frac{w_I N_I(\boldsymbol{\xi})}{W} = \frac{w_I N_I(\boldsymbol{\xi})}{\sum_{J=1}^N N_J(\boldsymbol{\xi}) w_J}, \quad (15)$$

where the B-spline functions $N_I(\boldsymbol{\xi})$ of degree p are defined by the knot-vectors on a parameter domain $\Omega_{\boldsymbol{\xi}} = [0, 1]^d$:

$$\Xi^i := \{\xi_1^i, \dots, \xi_{n_i+p+1}^i\}, \quad 0 = \xi_1^i \leq \xi_2^i \leq \xi_{n_i+p+1}^i = 1 \quad \text{and} \quad i = 1, \dots, d, \quad (16)$$

and n_i is the number of B-spline functions in each spatial direction.

B-spline basis functions in the parameter space span in several elements (knot spans), which makes numerical implementation more difficult. In order to use element-wise structures similar to the standard finite element method, B-spline basis functions are rewritten as a linear combination of the Bernstein polynomials $\mathbf{B}(\boldsymbol{\xi})$ defined on a parent element domain $[-1, 1]^d$, generating Bézier elements which have C^0 -continuity (see Fig. 2)

$$\mathbf{N}^e = \mathbf{C}^e \mathbf{B}(\boldsymbol{\xi}). \quad (17)$$

\mathbf{N}^e is a set of nb B-spline basis functions associated to the Bézier element, i.e., $\mathbf{N}^e = [N_1^e, \dots, N_{nb}^e]$. The localized extraction operator \mathbf{C}^e is constructed from the knot vector and is independent of control points as well as the B-spline basis functions. Similarly, NURBS basis functions within a

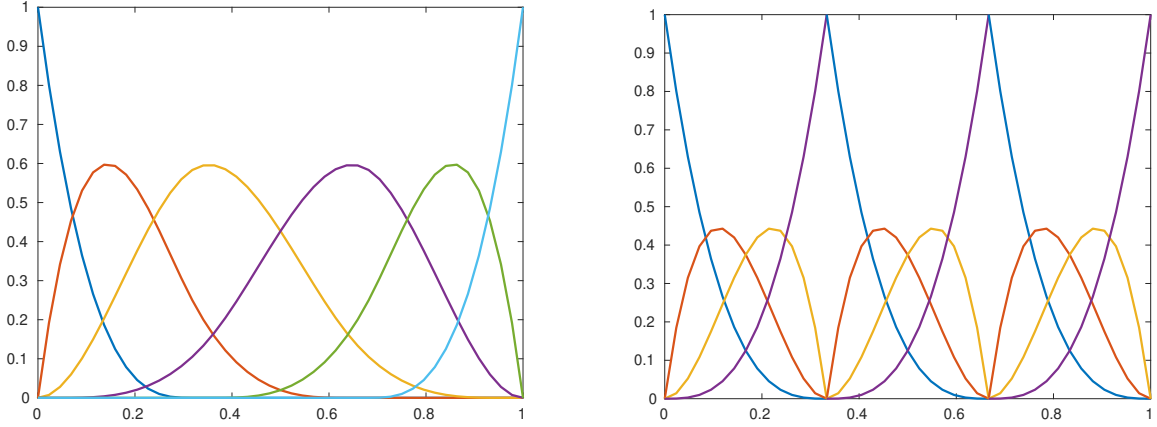


Figure 2: B-spline basis functions (left) and their corresponding Bernstein-Bézier representation (right).

Bézier element have the form:

$$\mathbf{R}^e(\boldsymbol{\xi}) = \frac{\mathbf{W}^e \mathbf{C}^e \mathbf{B}(\boldsymbol{\xi})}{\sum_{J=1}^{nb} w_J N_J^e(\boldsymbol{\xi})} = \frac{\mathbf{W}^e \mathbf{N}^e(\boldsymbol{\xi})}{W(\boldsymbol{\xi})}, \quad (18)$$

where \mathbf{W}^e is a diagonal matrix of weights. The implementation of IGA using the Bézier extraction allows the possibility of using existing routines in the finite element codes, i.e, assembly and post-processing.

For a unit cell discretized by nel Bézier elements as shown in Fig. 1(b), the equilibrium equation (4) has the following expression in matrix form

$$\mathbf{K} \boldsymbol{\chi}^{mn} = \mathbf{F}^{mn}, \quad (19)$$

where the global stiffness matrix \mathbf{K} and force vector \mathbf{F}^{mn} are assembled from corresponding element matrix and vector

$$\mathbf{k}^e = \int_{\Omega^e} \mathbf{B}^T \mathbf{C} \mathbf{B} d\Omega^e, \quad \mathbf{f}^{e,mn} = \int_{\Omega^e} \mathbf{B}^T \mathbf{C} \boldsymbol{\varepsilon}^{0,mn} d\Omega^e. \quad (20)$$

Herein, \mathbf{B} is the standard matrix of elastic strain operator in solid mechanics [43], and \mathbf{C} is the matrix of elasticity coefficient. The effective elasticity tensor is calculated from characteristic displacements:

$$C_{ijkl}^H = \frac{1}{|Y|} \sum_e \int_{\Omega^e}^{nel} [\boldsymbol{\varepsilon}^{0,ij} - \mathbf{B}\boldsymbol{\chi}^{ij}]^T \mathbf{C} [\boldsymbol{\varepsilon}^{0,kl} - \mathbf{B}\boldsymbol{\chi}^{kl}]. \quad (21)$$

5. Reduced order modelling

At each optimization iteration, the characteristic displacements $\boldsymbol{\chi}$ are obtained by solving the system of equations (19) and the computational cost involved in the inversion of stiffness matrix \mathbf{K} is expensive in large scale problems. We aim at reducing the finite dimensional space $V_0^h \subset H^1$ by

projecting the balance equation to subspace $\tilde{V}_0^h \subset V_0^h$ with lower dimension

$$\dim(\tilde{V}_0^h) = nb \ll \dim(V_0^h). \quad (22)$$

The task is to construct global ansatz functions $\theta_m(\mathbf{y})$ such that the subspace $\tilde{V}_0^h = \text{span}\{\theta_1, \dots, \theta_{nb}\}$, and solution fields in the reduced space are defined by

$$\chi^h(\mathbf{y}) \simeq \tilde{\chi}^h(\mathbf{y}) = \sum_m^{nb} \varphi_m \theta_m(\mathbf{y}). \quad (23)$$

The functions θ_m define the linear space \tilde{V}_0^h and are associated to the matrix of coefficients $\Phi \in \mathbb{R}^{N \times nb}$ by

$$\theta_m(\mathbf{y}) = \sum_n^N \Phi_{nm} R_n(\mathbf{y}), \quad (24)$$

where R_n are basis functions defined in (14). The balance equations (19) have the size of $nb \ll N$ in the subspace and are formed as

$$\tilde{\mathbf{K}} \tilde{\chi} = \tilde{\mathbf{F}}, \quad (25)$$

where $\chi = \Phi \tilde{\chi}$, $\tilde{\mathbf{K}} = \Phi^T \mathbf{K} \Phi$ and $\tilde{\mathbf{F}} = \Phi^T \mathbf{F}$.

The construction of the reduced basis follows the work by Gogu [17]. The key idea is to predict a new displacement solution and consequently a new topology by a set of solutions obtained from the previous iterations. We initialize the matrix Φ with vectors of coefficients ϕ_m calculated from the corresponding solutions χ_m (i.e., displacements associated to control points) in the first nb iterations. The first basis vector is given as

$$\phi_1 = \frac{\chi_1}{\|\chi_1\|}. \quad (26)$$

The next basis vector is computed by the Gram-Schmidt orthogonalization and normalization:

$$\tilde{\phi}_{m+1} = \chi_{m+1} - \sum_j^m \langle \chi_{m+1}, \phi_j \rangle \phi_j \quad (27)$$

$$\phi_{m+1} = \frac{\tilde{\phi}_{m+1}}{\|\tilde{\phi}_{m+1}\|}, \quad m = 1, \dots, (nb - 1).$$

Once the reduced basis is formed, a solution in the next iteration is obtained in the subspace of dimension nb and then transformed back to full space by using (25). In order to assess the accuracy of the solution obtained from the reduced basis, the following error measurement is suggested (see also [17])

$$error = \frac{\|\mathbf{K} \Phi \tilde{\chi} - \mathbf{F}\|}{\|\mathbf{F}\|} < tol. \quad (28)$$

If the error is acceptable, the optimization algorithm is conducted using the reduced solution. Otherwise, a full solution is calculated and used for the computations at the subsequent steps. After

each successful iteration, the reduced basis is enriched by adding the new accepted solution. The comparison of conventional optimization algorithms and those with reduced basis model is shown in Fig. 3. The two flowcharts have similar procedures except for the decision of using reduced solutions in subsequent steps (red box).

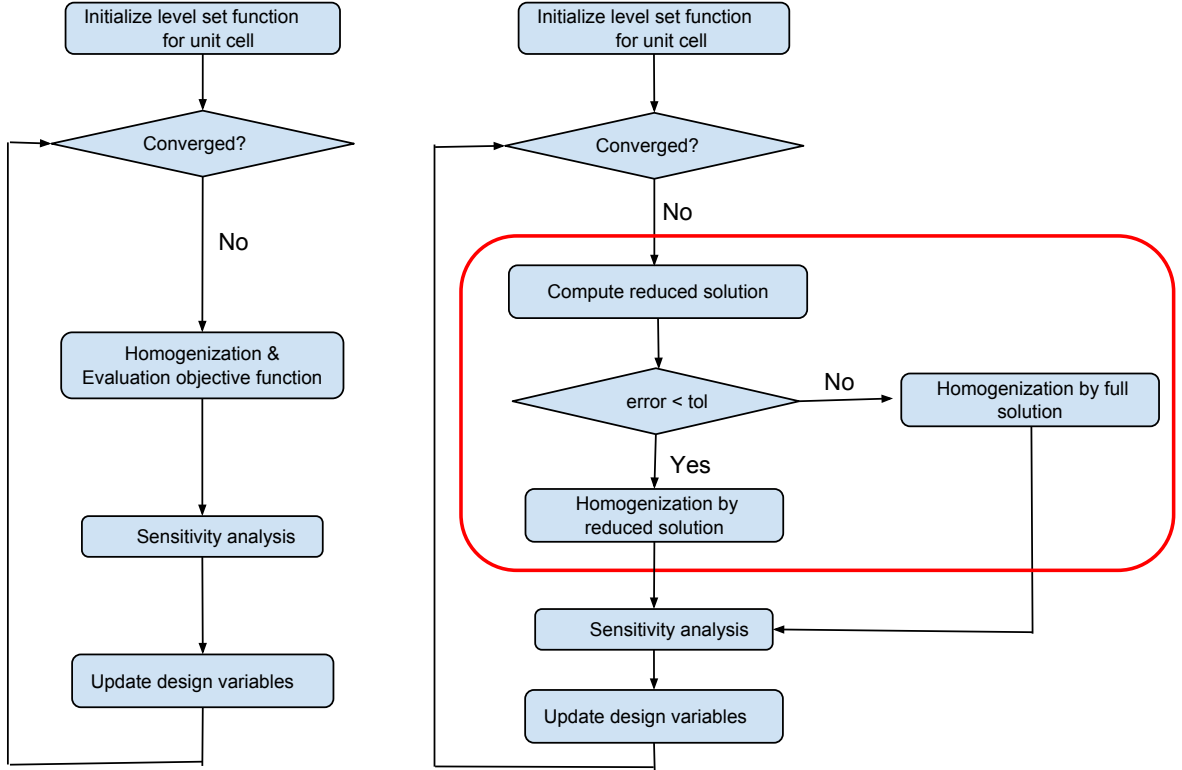


Figure 3: Microstructure topology optimization algorithm with and without reduced basis model.

This approach is similar to alternative projection-based methods, i.e., mode superposition, Ritz vectors method [44], or the proper orthogonal decomposition [45]. The original problem is solved for different values of the considered parameters in an offline stage and the pre-calculated solutions are then collected in order to construct a subspace. However, it is difficult to construct such parameter spaces in a topological shape optimization problem. The number of parameters needs to be large enough to represent all possibilities of shape or topology changes, which makes the reduced solutions inaccurate or difficult to obtain. Instead of using the offline strategy, the stored displacements from consecutive iterations during the optimization process are used here to construct the subspace, and a reduced solution obtained without solving the full system in the subsequent iteration is expected to satisfy the equilibrium equation.

6. Sensitivity analysis

Due to the gradient-based optimization algorithm which is used, it is necessary to find the derivatives of the objective function and constraints with respect to the design variables α_I . We follow the shape design sensitivity analysis by Choi et al. [46]. The shape boundary of the physical domain is considered as the design variable, and shape sensitivity analyzes the relation of shape boundary perturbations to the objective function or constraints. By representing the shape boundary by a zero level set function, the perturbations of the shape boundary become a dynamic evolution of the

level set function in time. The derivative of a domain functional with respect to shape can be replaced by the time derivative [38, 39]. In order to include the reduced solutions to the optimization algorithm, we define a general objective function for each component of the homogenized elastic tensor as follows

$$J(\tilde{\boldsymbol{\chi}}, \boldsymbol{\chi}, \mathbf{v}, \boldsymbol{\lambda}, \phi) = f(\tilde{\boldsymbol{\chi}}, \phi) + (a(\tilde{\boldsymbol{\chi}}, \mathbf{v}, \phi) - l(\mathbf{v}, \phi)) + \sum_m^{nb} (a(\boldsymbol{\chi}_m, \boldsymbol{\lambda}_m, \phi) - l(\boldsymbol{\lambda}_m, \phi)), \quad (29)$$

where

$$f(\tilde{\boldsymbol{\chi}}, \phi) = \int_Y (\varepsilon_{pq}^{0,ij} - \varepsilon_{pq}(\tilde{\boldsymbol{\chi}}^{ij})) C_{pqrs} (\varepsilon_{rs}^{0,kl} - \varepsilon_{rs}(\tilde{\boldsymbol{\chi}}^{kl})) \mathcal{H}(\phi) d\Omega, \quad (30)$$

and variational problems in the reduced sub-space \tilde{V}_0^h and in the finite dimensional space V_0^h are defined respectively as

$$\begin{aligned} a(\tilde{\boldsymbol{\chi}}, \mathbf{v}, \phi) &= \int_Y \varepsilon_{pq}(\tilde{\boldsymbol{\chi}}^{ij}) C_{pqrs} \mathcal{H}(\phi) \varepsilon_{rs}(\mathbf{v}) d\Omega \\ l(\mathbf{v}, \phi) &= \int_Y \varepsilon_{pq}^{0,ij} C_{pqrs} \mathcal{H}(\phi) \varepsilon_{rs}(\mathbf{v}) d\Omega \\ a(\boldsymbol{\chi}_m, \boldsymbol{\lambda}_m, \phi) &= \int_Y \varepsilon_{pq}(\boldsymbol{\chi}_m^{ij}) C_{pqrs} \mathcal{H}(\phi) \varepsilon_{rs}(\boldsymbol{\lambda}_m) d\Omega \\ l(\boldsymbol{\lambda}_m, \phi) &= \int_Y \varepsilon_{pq}^{0,ij} C_{pqrs} \mathcal{H}(\phi) \varepsilon_{rs}(\boldsymbol{\lambda}_m) d\Omega. \end{aligned} \quad (31)$$

The subscript m indicates the full solutions $\boldsymbol{\chi}_m$ were used to construct reduced basis $\boldsymbol{\phi}_m$. Shape derivatives of the objective function are given as

$$\begin{aligned} \dot{J} &= f(\dot{\tilde{\boldsymbol{\chi}}}, \phi) + f(\tilde{\boldsymbol{\chi}}, \dot{\phi}) + a(\dot{\tilde{\boldsymbol{\chi}}}, \mathbf{v}, \phi) + a(\tilde{\boldsymbol{\chi}}, \dot{\mathbf{v}}, \phi) + a(\tilde{\boldsymbol{\chi}}, \mathbf{v}, \dot{\phi}) - l(\dot{\mathbf{v}}, \phi) - l(\mathbf{v}, \dot{\phi}) \\ &+ \sum_m^{nb} \left(a(\dot{\boldsymbol{\chi}}_m, \boldsymbol{\lambda}_m, \phi) + a(\boldsymbol{\chi}_m, \dot{\boldsymbol{\lambda}}_m, \phi) + a(\boldsymbol{\chi}_m, \boldsymbol{\lambda}_m, \dot{\phi}) - l(\dot{\boldsymbol{\lambda}}_m, \phi) - l(\boldsymbol{\lambda}_m, \dot{\phi}) \right), \end{aligned} \quad (32)$$

where the terms containing time derivatives, for example of the homogenized elastic tensor, have forms as

$$\begin{aligned} f(\tilde{\boldsymbol{\chi}}, \dot{\phi}) &= \int_Y (\varepsilon_{pq}^{0,ij} - \varepsilon_{pq}(\tilde{\boldsymbol{\chi}}^{ij})) C_{pqrs} (\varepsilon_{rs}^{0,kl} - \varepsilon_{rs}(\tilde{\boldsymbol{\chi}}^{kl})) \delta(\phi) |\nabla \phi| V_n d\Omega, \\ f(\dot{\tilde{\boldsymbol{\chi}}}, \phi) &= \int_Y -2 \varepsilon_{pq}(\dot{\tilde{\boldsymbol{\chi}}}^{ij}) C_{pqrs} (\varepsilon_{rs}^{0,kl} - \varepsilon_{rs}(\tilde{\boldsymbol{\chi}}^{kl})) \mathcal{H}(\phi) d\Omega, \end{aligned} \quad (33)$$

$\delta(\circ) = \mathcal{H}'(\circ)$ being the Dirac delta function. To avoid calculating the time derivative of the characteristic displacement $\dot{\tilde{\boldsymbol{\chi}}}$ in (32), the following adjoint equation is established and solved for \mathbf{v}

in general.

$$f(\tilde{\boldsymbol{\chi}}, \phi) + a(\tilde{\boldsymbol{\chi}}, \mathbf{v}, \phi) = 0. \quad (34)$$

In fact (34) is a self-adjoint problem and is satisfied if the test function \mathbf{v} is properly selected such that

$$\varepsilon_{rs}(\mathbf{v}) = 2 \left(\varepsilon_{rs}^{0,kl} - \varepsilon_{rs}(\tilde{\boldsymbol{\chi}}^{kl}) \right). \quad (35)$$

All the terms containing $\dot{\boldsymbol{\lambda}}_m$ can be eliminated since the following relations hold true

$$a(\boldsymbol{\chi}_m, \dot{\boldsymbol{\lambda}}_m, \phi) = l(\dot{\boldsymbol{\lambda}}_m, \phi) \quad \forall \boldsymbol{\lambda}_m \in V_0^h, \quad m = 1, \dots, nb. \quad (36)$$

If the standard solution is used instead of reduced solutions, i.e., $\tilde{\boldsymbol{\chi}} \rightarrow \boldsymbol{\chi}$, the residual is defined by

$$r(\tilde{\boldsymbol{\chi}}, \dot{\mathbf{v}}, \phi) = a(\tilde{\boldsymbol{\chi}}, \dot{\mathbf{v}}, \phi) - l(\dot{\mathbf{v}}, \phi) = 0, \quad \forall \dot{\mathbf{v}} \in V_0^h. \quad (37)$$

In this case, shape derivatives of the homogenized elastic tensor are

$$\frac{\partial J}{\partial \tau} = \frac{\partial C_{ijkl}^H}{\partial \tau} = - \int_Y (\varepsilon_{pq}^{0,ij} - \varepsilon_{pq}(\boldsymbol{\chi}^{ij})) C_{pqrs} (\varepsilon_{rs}^{0,kl} - \varepsilon_{rs}(\boldsymbol{\chi}^{kl})) \delta(\phi) |\nabla \phi| V_n d\Omega. \quad (38)$$

If a reduced solution $\tilde{\boldsymbol{\chi}}$ is used, the residual is non-zero and written as

$$r(\tilde{\boldsymbol{\chi}}, \dot{\mathbf{v}}, \phi) = r(\tilde{\boldsymbol{\chi}}, \sum_m^{nb} \varphi_m \dot{\boldsymbol{\theta}}_m, \phi) = \sum_m^{nb} \varphi_m r(\tilde{\boldsymbol{\chi}}, \dot{\boldsymbol{\theta}}_m, \phi). \quad (39)$$

To eliminate the quantity $\dot{\boldsymbol{\chi}}_m$ in (32), the following adjoint equations are formed for each set of the balance equations

$$a(\dot{\boldsymbol{\chi}}_m, \boldsymbol{\lambda}_m, \phi) + \varphi_m r(\tilde{\boldsymbol{\chi}}, \dot{\boldsymbol{\theta}}_m, \phi) = 0, \quad m = 1, \dots, nb. \quad (40)$$

As the global ansatz function θ_m is constructed from the standard solutions χ in the finite-dimensional space V_0^h (see Eq. (24), (26)-(27)) and as the bilinear form $a(\circ, \circ)$ is symmetric in its arguments, the adjoint equation finally has the form as

$$a(\boldsymbol{\lambda}_m, \dot{\boldsymbol{\chi}}_m, \phi) + \varphi_m r(\tilde{\boldsymbol{\chi}}, \dot{\boldsymbol{\chi}}_m, \phi) = 0, \quad m = 1, \dots, nb \quad (41)$$

and solved for the adjoint variables $\boldsymbol{\lambda}_m$. The final expression of the sensitivity is

$$\dot{J} = f(\tilde{\boldsymbol{\chi}}, \dot{\phi}) + a(\tilde{\boldsymbol{\chi}}, \mathbf{v}, \dot{\phi}) - l(\mathbf{v}, \dot{\phi}) + \sum_m^{nb} \left(a(\boldsymbol{\chi}_m, \boldsymbol{\lambda}_m, \dot{\phi}) - l(\boldsymbol{\lambda}_m, \dot{\phi}) \right) \quad (42)$$

in which adjoint variables \mathbf{v} and $\boldsymbol{\lambda}_m$ are obtained from the self-adjoint problem (35) and (41) respectively. If the Hamilton-Jacobi equation is replaced by an original differential equation (9), any integral function involving the normal velocity component

$$\dot{j} = \frac{\partial J(\circ, \phi)}{\partial \tau} = g(\circ, \dot{\phi}) = \int_Y (\circ) \delta(\phi) |\nabla \phi| V_n d\Omega \quad (43)$$

can be written as

$$\frac{\partial J(\circ, \phi)}{\partial \tau} = \sum_{I=1}^{ncp} \left(\int_Y (\circ) \delta(\phi) R_I(\mathbf{x}) d\Omega \right) \cdot \dot{\alpha}_I. \quad (44)$$

Additionally, the time derivative of the objective function J can be obtained by applying the chain rule

$$\frac{\partial J(\circ, \phi)}{\partial \tau} = \sum_{I=1}^{ncp} \frac{\partial J(\circ, \phi)}{\partial \alpha_I} \frac{\partial \alpha_I}{\partial \tau}. \quad (45)$$

By comparing (45) and (44), the sensitivity analysis of the objective function with respect to the design variable α_I is

$$\frac{\partial J(\circ, \phi)}{\partial \alpha_I} = \int_Y (\circ) \delta(\phi) R_I(\mathbf{x}) d\Omega. \quad (46)$$

The sensitivity analysis of volume constraint is given as

$$\frac{\partial V}{\partial \alpha_I} = \int_Y \delta(\phi) R_I(\mathbf{x}) d\Omega. \quad (47)$$

7. Numerical examples

The homogenization method detailed in [Section 2](#) allows to predict the macroscopic properties of composites from a unit cell geometry. Designing the behavior of composite material is replaced by designing a unit cell such that the effective properties meet requirements. Seeking for auxetic materials turns into designing the effective elasticity tensor having negative Poisson's ratio. Therefore, we can assume that the target properties of material are given, and the optimization process is to search for the unit cell geometries such that the difference between effective properties and target properties is minimized.

$$\begin{aligned} \min \quad & J_1 = \frac{1}{2} \sum_{i,j,k,l=1}^d \omega_{ijkl} \times (C_{ijkl} - C_{ijkl}^*)^2 \\ \text{s.t.} \quad & \begin{cases} a(\mathbf{x}, \mathbf{v}, \phi) = l(\mathbf{v}, \phi) & \text{(equilibrium equation)} \\ V(\phi) = \int_Y \mathcal{H}(\phi) d\Omega \leq v_f & \text{(volume constraint)} \\ \alpha_{\min} \leq \alpha_i \leq \alpha_{\max} \quad (i = 1, 2, \dots, N) & \text{(design variable constraint)} \end{cases} \end{aligned} \quad (48)$$

where C_{ijkl}^* are the components of the target elasticity matrix which has the following form in the two-dimensional dimension

$$\mathbf{C}^* = \begin{bmatrix} C_{1111}^* & C_{1122}^* & 0 \\ C_{1122}^* & C_{2222}^* & 0 \\ 0 & 0 & C_{1212}^* \end{bmatrix}, \quad (49)$$

and ω_{ijkl} are weighting factors used in the least-square function. The bilinear energy form $a(\boldsymbol{\chi}, \mathbf{v}, \phi)$ and linear load form $l(\mathbf{v}, \phi)$ are defined in (10).

We first consider 2D unit cells subjected to plane stress conditions and discretized with an IGA mesh with 60×60 order $p = 2$ polynomial Bézier elements. The solid part in the unit cell is constituted by an isotropic material having Young’s modulus $E = 1.0$ GPa and Poisson’s ratio $\nu = 0.3$. The target elasticity components are set to $C_{1111}^* = C_{2222}^* = 0.1$, $C_{1122}^* = -0.05$ which ensures that the final configuration has negative Poisson’s ratio. We set the weighting factors $\omega_{1111} = \omega_{2222} = 0.01$, $\omega_{1122} = 0.5$. For a level set function initialized with expansion coefficients, the upper bound $\alpha_{\max} = \max\{\alpha_I^0\}$ and lower bound $\alpha_{\min} = \min\{\alpha_I^0\}$ are chosen in the subsequent iterations. We use the method of moving asymptotic (MMA) [47] to update the design variables. Orthotropic materials are obtained by considering the geometry symmetry of square unit cells, the expansion coefficients α_I in one-quarter of the unit cell are updated and the remaining configurations are obtained from the reflectional symmetry.

Optimal solutions corresponding to different initial configurations, target volumes are given in Fig. 4. Despite the initial configurations consist of simple circles, the complex shapes with sharp boundaries and thin ribs occur in the designs. There is no gray area or blur boundaries, the solid and void interfaces are clear. The verification or fabrication procedure can be directly performed for those final designs. These advantages of features of level set methods are highly preferable. Final shapes of unit cells are different due to the fact that the optimization algorithm (MMA) is a local optimizer. To summarize, the generated unit cells with negative Poisson’s ratios are obtained and similar to well-known auxetic structures: anti-tetra-chiral structures [48] (see Fig. 4(c)), re-entrant structures [49] (see Fig. 4(b, d)), or auxetic microstructures obtained with SIMP [50] (see Fig. 4(a, e)).

The volume fraction constraints significantly affect the final designs. In fact, negative Poisson’s ratio in materials is created by a mechanism with trusses or beams connected through hinges. These structures induce perpendicular motions among components by bending or rotating at the hinges. As much material is removed, a higher possibility of thin layers is produced. The amount of material removed also drives elastic stiffness of unit cells, this is a trade-off between the effective Young’s modulus and negative Poisson’s ratios in auxetic microstructure optimization. Softer materials have higher auxetic effects and vice-versa.

Geometries of the unit cell are plotted as selected iterations shown in Fig. 5 illustrating topology change during the optimization process. At the beginning, material is removed to satisfy the volume constraint and the objective function oscillates significantly within the first 20 iterations. Topology changes mainly take place in this material removal process. Dynamic moving of boundaries with merging and splitting allows to remove existing holes or create new holes, increasing the design flexibility of shape and topology. Solid domains link together and meaningless features like islands are eliminated while the objective function values are reducing gradually. After 125 iterations, the objective function is kept unchanged and Poisson’s ratios are minimized.

We next investigate the influence of the reduced basis approach to the convergence rate and final design. The same initial configuration is considered but the algorithm with reduced order model (as shown in Fig. 3) is used in this example. A reduced basis with size $nb = 12$ is constructed and enriched during the optimization process. Reduced solutions are accepted and used in further calculation steps if the residual error is smaller than a threshold $tol = 0.01$ for all test cases ($mn = 11, 22, 12$) simultaneously. As shown in Fig. 6, the objective function varies dramatically in the first few iterations along with the large change in shape and topology due to material removal. These imply that the reduced solutions, generated by a set of different configurations, will not satisfy the condition (28), and full solutions are required to be computed. When the objective function values are gradually decreasing, a set of similar geometries and corresponding basis vectors enrich

the reduced basis sufficiently, this subspace enables to produce reduced solutions which are accurate enough to proceed with the next calculation steps. The blue squares indicate that the optimization algorithm applies the reduced model order successfully and computational burden of solving the original system is eliminated by inverting the systems with small size, i.e., $nb = 12$.

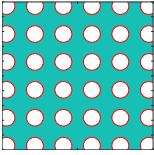
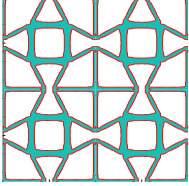
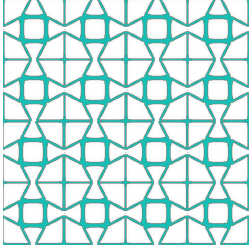
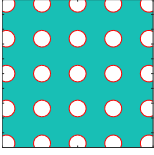
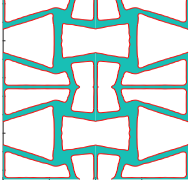
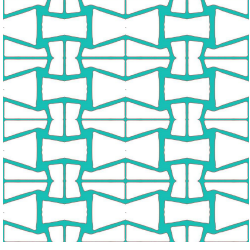
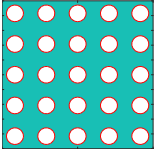
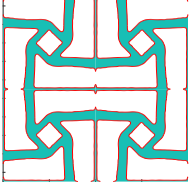
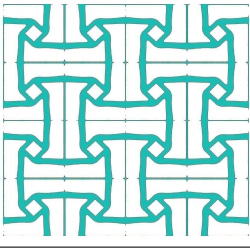
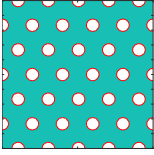
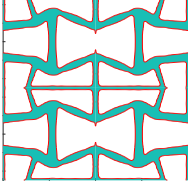
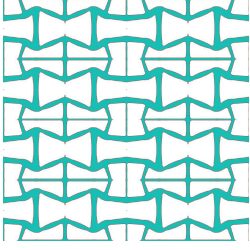
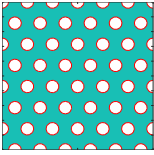
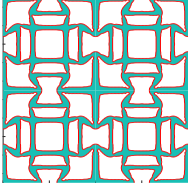
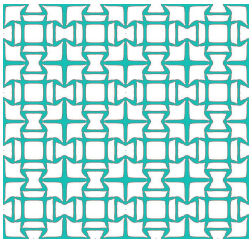
Initial design	Optimized unit cell	2×2 repeated unit cells	Effective property & volume fraction
(a) 			$\mathbf{C}^H = \begin{bmatrix} 0.0658 & -0.0372 & 0 \\ -0.0372 & 0.0658 & 0 \\ 0 & 0 & 0.0020 \end{bmatrix}$ $V_f = 0.275$ $\nu_{xy} = \nu_{yx} = -0.565$
(b) 			$\mathbf{C}^H = \begin{bmatrix} 0.0921 & -0.0430 & 0 \\ -0.0430 & 0.05 & 0 \\ 0 & 0 & 0.0014 \end{bmatrix}$ $V_f = 0.275$ $\nu_{xy} = -0.466, \nu_{yx} = -0.860$
(c) 			$\mathbf{C}^H = \begin{bmatrix} 0.046 & -0.039 & 0 \\ -0.039 & 0.046 & 0 \\ 0 & 0 & 0.0012 \end{bmatrix}$ $V_f = 0.3$ $\nu_{xy} = \nu_{yx} = -0.830$
(d) 			$\mathbf{C}^H = \begin{bmatrix} 0.1094 & -0.0419 & 0 \\ -0.0419 & 0.052 & 0 \\ 0 & 0 & 0.0018 \end{bmatrix}$ $V_f = 0.3$ $\nu_{xy} = -0.383, \nu_{yx} = -0.805$
(e) 			$\mathbf{C}^H = \begin{bmatrix} 0.0840 & -0.0507 & 0 \\ -0.0507 & 0.0840 & 0 \\ 0 & 0 & 0.004 \end{bmatrix}$ $V_f = 0.35$ $\nu_{xy} = \nu_{yx} = -0.603$

Figure 4: Influence of initial configurations and volume fraction to final designs.

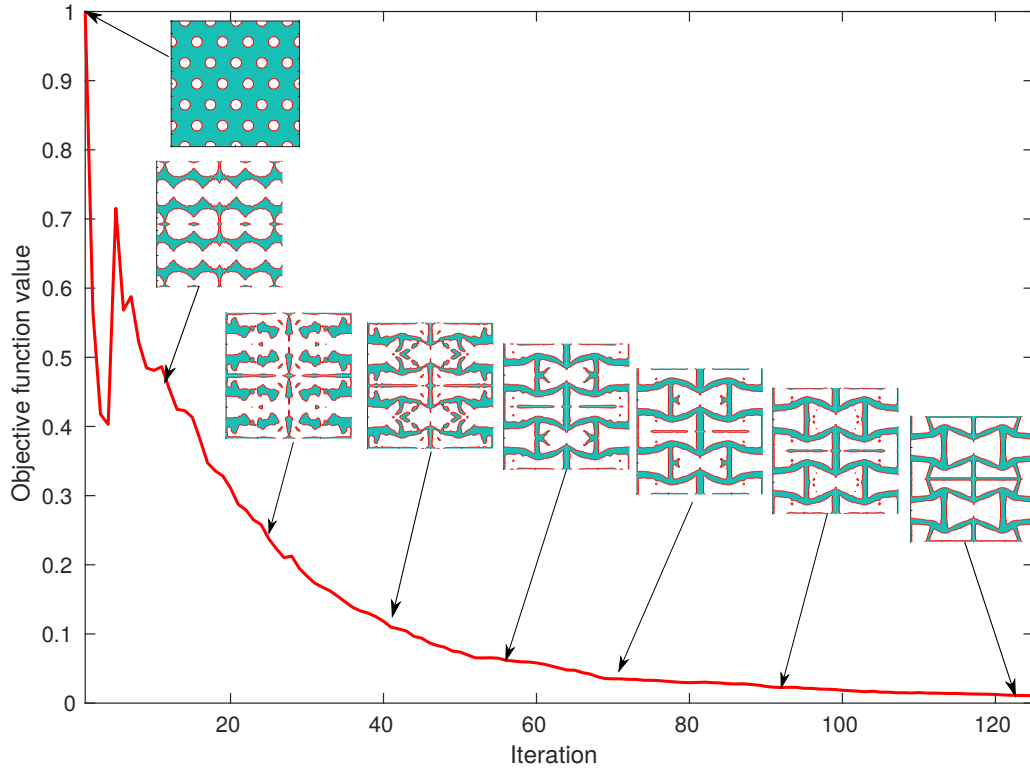


Figure 5: Convergence of the objective function.

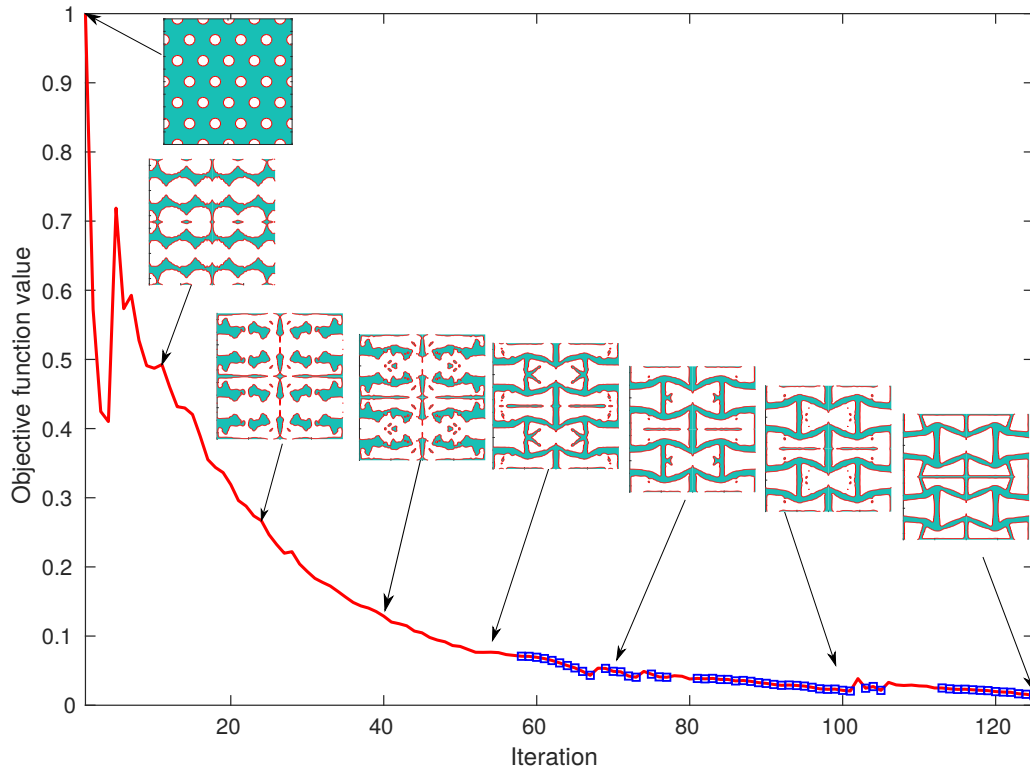


Figure 6: Convergence of the objective function by using the algorithm with reduced order model in Fig. 3 (right). Blue squares indicate the reduced solutions are used.

We further design three-dimensional metamaterials with negative Poisson’s ratio by considering a cubic unit cell and investigate the efficiency of using reduced modeling when the size of problems is increased. Design domains are discretized with 40^3 quadratic Bézier elements thus leading to moderately large models which are time consuming if balance equations are solved in the finite dimensional space V_0^h . We use a reduced basis with $nb = 12$ and errors smaller than $tol = 0.01$ to decide whether the reduced solutions are accurate and subsequently employed to advance a new topology. Figure 7 provides optimized structures and corresponding homogenized elastic tensors which are results of optimization algorithm with reduced modeling. Designed geometries exhibit auxetic effect if the structures are under compression or tension. Due to the nature of gradient-based algorithms which accept local optimums, final results can be different although the same target elastic tensor is set for the objective functions.

The plot of convergence in Fig. 8 indicates iterations at which reduced modeling applied successfully. A similar behavior of the algorithm as shown in the two-dimensional problem (cf. Fig. 6) is also observed in this 3D example. Significant changes topology and shapes lead to the reduced basis at the initial stage can not produce accurate solutions. Afterwards, the shapes and topology advance gradually resulting on similar geometries produced and the reduced basis constructed from full solutions are able to reproduce accurate solutions used in next consecutive steps.

The computation time and number of iterations required in the 3D examples are summarized in Tab. 1. We simulate examples in similar settings but with and without using the reduced order model. The optimized structures of each simulation are slightly different (and are not shown here) due to the local optimum characteristic of the optimizer. We purposely eliminate all possible instabilities and keep the optimizer conservative by using small moving stepsizes [51], hence, the number of iterations is relatively large in all numerical examples. In this way, we can have adequate comparisons between the two algorithms and can emphasize the outperformance of the reduced order technique. The total CPU time required in full model is larger although fewer number of iterations are used. In such large scale problems, the time for stiffness matrix assembly is negligible and the computational cost of solving the system of equation is dominant. If reduced solutions are accurate enough to advance new topology in the consecutive step, the computational cost of solving original large equations is eliminated by determining solutions of system with small size of $nb \times nb$ and a speed-up of factor 6.0 in solving the equation is achieved.

Unit cells	Full model		Reduced order model		
	Number of iterations	CPU time (in hour)	Number of iterations	Number of iterations using reduced solution	CPU time (in hour)
a	420	12.25	624	532	10.25
b	672	19.3	685	628	10.9
c	525	16.6	578	503	11.4
d	480	15.2	472	403	8.9

Table 1: Computation time of the 3D examples with and without using reduced order modelling.

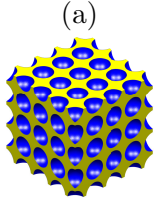
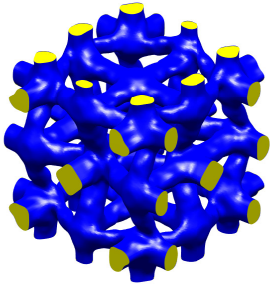
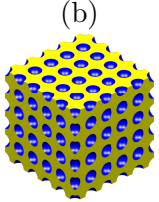
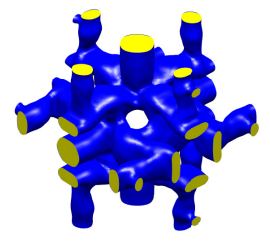
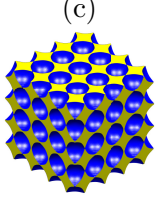
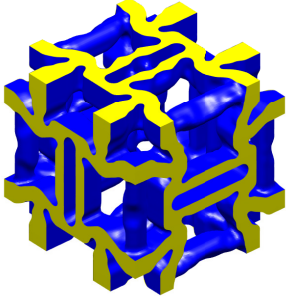
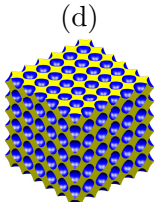
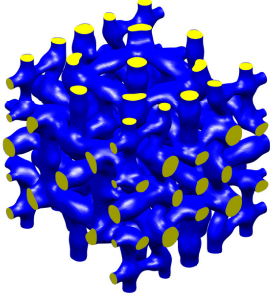
Initial design	Optimized unit cell	Effective property \mathbf{C}^H & volume fraction
(a) 		$0.1 \times \begin{bmatrix} 0.29 & -0.11 & -0.095 & 0 & 0 & 0 \\ -0.11 & 0.38 & -0.063 & 0 & 0 & 0 \\ -0.095 & -0.063 & 0.50 & 0 & 0 & 0 \\ 0 & 0 & 0 & 0.04 & 0 & 0 \\ 0 & 0 & 0 & 0 & 0.03 & 0 \\ 0 & 0 & 0 & 0 & 0 & 0.03 \end{bmatrix}$ $V_f = 0.225$
(b) 		$0.1 \times \begin{bmatrix} 0.34 & -0.077 & -0.048 & 0 & 0 & 0 \\ -0.077 & 0.4 & -0.053 & 0 & 0 & 0 \\ -0.048 & -0.053 & 0.27 & 0 & 0 & 0 \\ 0 & 0 & 0 & 0.016 & 0 & 0 \\ 0 & 0 & 0 & 0 & 0.013 & 0 \\ 0 & 0 & 0 & 0 & 0 & 0.017 \end{bmatrix}$ $V_f = 0.25$
(c) 		$0.1 \times \begin{bmatrix} 0.5 & -0.086 & -0.083 & 0 & 0 & 0 \\ -0.086 & 0.65 & -0.09 & 0 & 0 & 0 \\ -0.083 & -0.09 & 0.61 & 0 & 0 & 0 \\ 0 & 0 & 0 & 0.046 & 0 & 0 \\ 0 & 0 & 0 & 0 & 0.047 & 0 \\ 0 & 0 & 0 & 0 & 0 & 0.052 \end{bmatrix}$ $V_f = 0.3$
(d) 		$0.1 \times \begin{bmatrix} 0.44 & -0.069 & -0.092 & 0 & 0 & 0 \\ -0.069 & 0.51 & -0.012 & 0 & 0 & 0 \\ -0.092 & -0.012 & 0.61 & 0 & 0 & 0 \\ 0 & 0 & 0 & 0.038 & 0 & 0 \\ 0 & 0 & 0 & 0 & 0.042 & 0 \\ 0 & 0 & 0 & 0 & 0 & 0.05 \end{bmatrix}$ $V_f = 0.3$

Figure 7: Influence of initial configurations and volume fractions to final designs in three-dimensional metamaterials design.

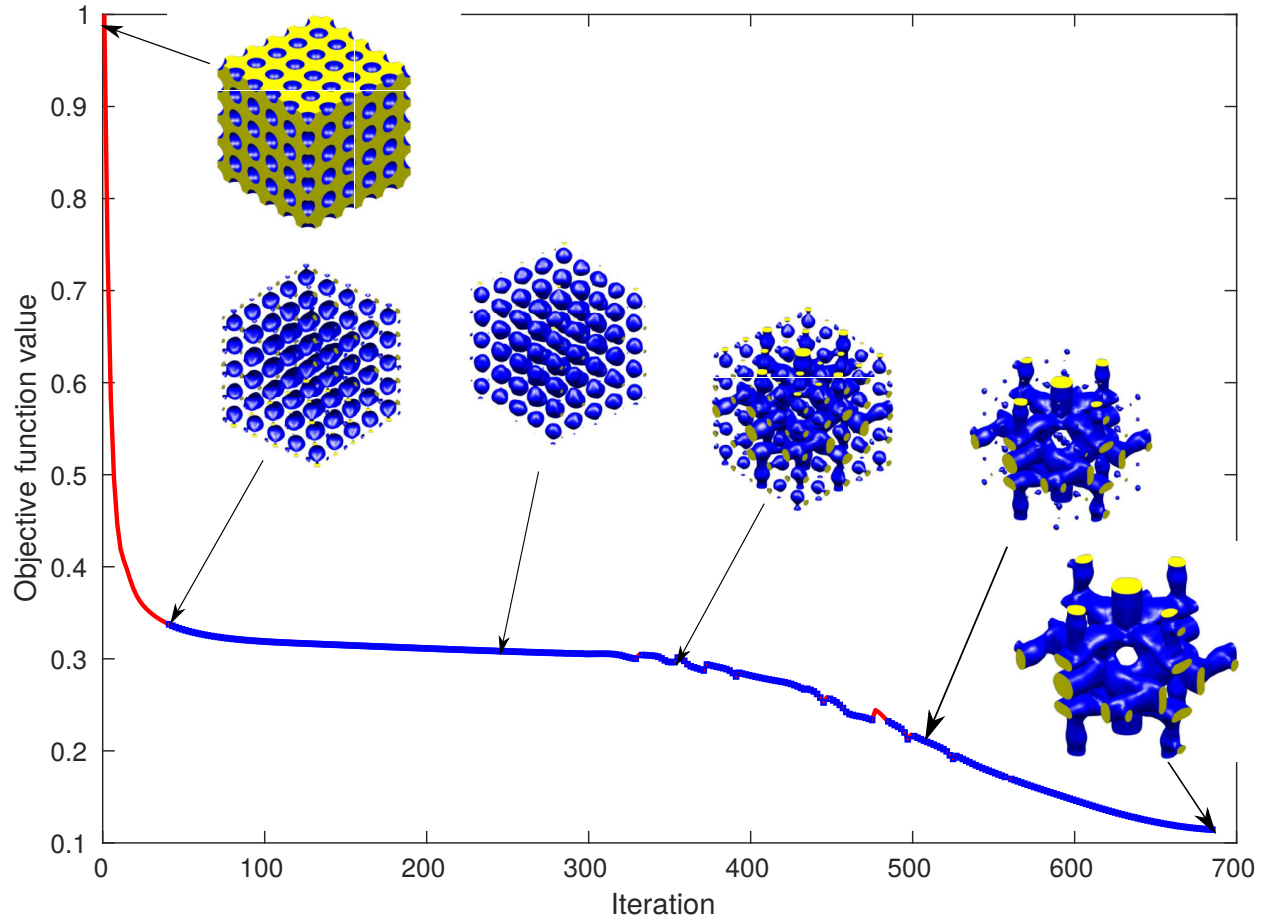


Figure 8: Convergence of the objective function (of the unit cell (b) in Fig. 7) by using the algorithm with reduced order modeling. Blue squares indicate the reduced solutions are used.

The feasibility of using reduced solutions in shape and topology optimization can trace back to reduced order models using the offline strategy. In these approaches, a set of parameters can represent the geometry adjustment, and pre-calculated solutions of the model are obtained by evaluating at selected parameter values. It is noted that when the variation of parameters does not result in the enormous change of geometry shape or topology, this allows the reduced basis to generate accurate solutions. In this current work, a similar idea for constructing the reduced basis is employed. Indeed, the stored solutions obtained from geometries are used to construct the reduced subspace. The amount of difference in geometries decides the enrichment level of the reduced basis and the accuracy of reduced solutions. The method is practical since minor changes in geometries always appear after several iterations (see Fig. 6 and Fig. 8).

8. Conclusion

Material microstructures with negative effective Poisson's ratio have been designed by topology optimization. Asymptotic homogenization method and sensitivity analysis of the effective elasticity tensor was revised and numerically implemented by isogeometric analysis with Bézier extraction. Geometries of the unit cell were represented by a parameterized level set function which allows flexible changes in shape and topology designs, and optimized structures having clear boundaries in order to be able to make prototypes with 3D printers directly. A reduced order modeling combined

with topology optimization was introduced to improve the computational efficiency in solving the linear system of equations. The numerical results show that such a combination are beneficial in topology optimization and could be extended to other physical problems such as improving electrical coefficients, or negative thermal expansion materials.

References

References

- [1] R. Lakes. Advances in negative poisson's ratio materials. *Advanced Materials*, 5(4):293–296, apr 1993.
- [2] K. E. Evans and A. Alderson. Auxetic materials: Functional materials and structures from lateral thinking! *Advanced Materials*, 12(9):617–628, 2000.
- [3] Y. M. Xie and G. P. Steven. A simple evolutionary procedure for structural optimization. Technical Report 5, 1993.
- [4] Y. M. Xie and G. P. Steven. Basic Evolutionary Structural Optimization. In *Evolutionary Structural Optimization*, pages 12–29. Springer London, London, 1997.
- [5] M. P. Bendsøe and O. Sigmund. Material interpolation schemes in topology optimization. *Archive of Applied Mechanics*, 69(9-10):635–654, 1999.
- [6] O. Sigmund. Materials with prescribed constitutive parameters: An inverse homogenization problem. *International Journal of Solids and Structures*, 31(17):2313–2329, 1994.
- [7] Ulrik Darling Larsen, O Signund, and S Bouwsta. Design and fabrication of compliant micromechanisms and structures with negative Poisson's ratio. *Journal of Microelectromechanical Systems*, 6(2):99–106, 1997.
- [8] G. Allaire, F. Jouve, and A. M. Toader. A level-set method for shape optimization. *Comptes Rendus Mathématique*, 334(12):1125–1130, jan 2002.
- [9] G. Allaire, F. Jouve, and G. Michailidis. Thickness control in structural optimization via a level set method. *Structural and Multidisciplinary Optimization*, pages 1–34, 2016.
- [10] G. Allaire and G. Michailidis. Modal basis approaches in shape and topology optimization of frequency response problems. *International Journal for Numerical Methods in Engineering*, pages n/a–n/a, 2017.
- [11] P. Vogiatzis, S. Chen, X. Wang, T. Li, and L. Wang. Topology optimization of multi-material negative Poisson's ratio metamaterials using a reconciled level set method. *Computer-Aided Design*, 83:15–32, 2017.
- [12] M. Y. Wang and X. Wang. “Color” level sets: a multi-phase method for structural topology optimization with multiple materials. *Computer Methods in Applied Mechanics and Engineering*, 193(6–8):469–496, 2004.
- [13] O. Amir, M. Stolpe, and O. Sigmund. Efficient Reanalysis Procedures in Structural Topology Optimization. *Department of Mathematics*, PhD(March):155, 2011.

- [14] S. Wang, E. de Sturler, and G. H. Paulino. Large-scale topology optimization using preconditioned Krylov subspace methods with recycling. *International Journal for Numerical Methods in Engineering*, 69(12):2441–2468, mar 2007.
- [15] L. Xia and P. Breitkopf. A reduced multiscale model for nonlinear structural topology optimization. *Computer Methods in Applied Mechanics and Engineering*, 280:117–134, 2014.
- [16] J. A. Hernández, J. Oliver, A. E. Huespe, M. A. Caicedo, and J. C. Cante. High-performance model reduction techniques in computational multiscale homogenization. *Computer Methods in Applied Mechanics and Engineering*, 276:149–189, 2014.
- [17] C. Gogu. Improving the efficiency of large scale topology optimization through on-the-fly reduced order model construction. *International Journal for Numerical Methods in Engineering*, 101(4):281–304, 2015.
- [18] T. J.R. Hughes, J. A. Cottrell, and Y. Bazilevs. Isogeometric analysis: CAD, finite elements, NURBS, exact geometry and mesh refinement. *Computer Methods in Applied Mechanics and Engineering*, 194(39-41):4135–4195, oct 2005.
- [19] J. A. Cottrell, T. J. R. Hughes, and Y. Bazilevs. *Isogeometric Analysis: Toward Integration of CAD and FEA*. Wiley, 2009.
- [20] Y. Wang and D. J. Benson. Isogeometric analysis for parameterized LSM-based structural topology optimization. *Computational Mechanics*, 57(1):19–35, 2016.
- [21] G. Costa, M. Montemurro, and J. Pailhès. Minimum length scale control in a NURBS-based SIMP method. *Computer Methods in Applied Mechanics and Engineering*, may 2019.
- [22] J. Gao, H. Xue, L. Gao, and Z. Luo. Topology optimization for auxetic metamaterials based on isogeometric analysis. *Computer Methods in Applied Mechanics and Engineering*, 352:211–236, 2019.
- [23] A. Manzoni, F. Salmoiraghi, and L. Heltai. Reduced Basis Isogeometric Methods (RB-IGA) for the real-time simulation of potential flows about parametrized NACA airfoils. *Computer Methods in Applied Mechanics and Engineering*, 284:1147–1180, 2015.
- [24] S. Zhu, L. Dedè, and A. Quarteroni. Isogeometric analysis and proper orthogonal decomposition for the acoustic wave equation. *ESAIM: Mathematical Modelling and Numerical Analysis*, 51(4):1197–1221, 2017.
- [25] A. Ammar, A. Huerta, F. Chinesta, E. Cueto, and A. Leygue. Parametric solutions involving geometry: A step towards efficient shape optimization. *Computer Methods in Applied Mechanics and Engineering*, 268:178–193, 2013.
- [26] L. Chamoin and H. P. Thai. Certified real-time shape optimization using isogeometric analysis, PGD model reduction, and a posteriori error estimation. *International Journal for Numerical Methods in Engineering*, (February):151–176, 2019.
- [27] J. D. Eshelby. The Determination of the Elastic Field of an Ellipsoidal Inclusion, and Related Problems, 1957.
- [28] T. Mori and K. Tanaka. Average stress in matrix and average elastic energy of materials with misfitting inclusions. *Acta Metallurgica*, 21(5):571–574, may 1973.

- [29] R. Hill. A self-consistent mechanics of composite materials. *Journal of the Mechanics and Physics of Solids*, 13(4):213–222, aug 1965.
- [30] J. Hohe and W. Becker. An energetic homogenisation procedure for the elastic properties of general cellular sandwich cores. *Composites Part B:Engineering*, 32(3):185–197, 2001.
- [31] Q. Yang and W. Becker. A comparative investigation of different homogenization methods for prediction of the macroscopic properties of composites. *Computer Modeling in Engineering and Sciences*, 6:319–332, 2004.
- [32] E. Sanchez-Palencia. Homogeneization in mechanics A survey of solved and open problems. *REND. SEM. MAT.*, 44(1):1–46, 1986.
- [33] W. Zhang, G. Dai, F. Wang, S. Sun, and H. Bassir. Using strain energy-based prediction of effective elastic properties in topology optimization of material microstructures. *Acta Mechanica Sinica/Lixue Xuebao*, 23(1):77–89, 2007.
- [34] J. Guedes and N. Kikuchi. Preprocessing and postprocessing for materials based on the homogenization method with adaptive finite element methods. *Computer Methods in Applied Mechanics and Engineering*, 83(2):143–198, oct 1990.
- [35] X. Zhuang, Q. Wang, and H. Zhu. A 3D computational homogenization model for porous material and parameters identification. *Computational Materials Science*, 96, Part B:536–548, 2015.
- [36] F. Fantoni, A. Bacigalupo, and M. Paggi. Multi-field asymptotic homogenization of thermopiezoelectric materials with periodic microstructure. *International Journal of Solids and Structures*, 120:31–56, 2017.
- [37] B. Hassani and E. Hinton. *Homogenization and structural topology optimization: theory, practice and software*. Springer Science & Business Media, 1998.
- [38] M. Y. Wang, X. Wang, and D. Guo. A level set method for structural topology optimization. *Computer Methods in Applied Mechanics and Engineering*, 192(1–2):227–246, 2003.
- [39] G. Allaire, F. Jouve, and A. Toader. Structural optimization using sensitivity analysis and a level-set method. *Journal of Computational Physics*, 194(1):363–393, 2004.
- [40] S. Osher and R. Fedkiw. *Level Set Methods and Dynamic Implicit Surfaces*, volume 153. Springer, 2003.
- [41] T. Belytschko, S. P. Xiao, and C. Parimi. Topology optimization with implicit functions and regularization. *International Journal for Numerical Methods in Engineering*, 57(8):1177–1196, jun 2003.
- [42] M. J. Borden, M. A. Scott, J. A. Evans, and T. J. R. Hughes. Isogeometric finite element data structures based on Bézier extraction of NURBS. *International Journal for Numerical Methods in Engineering*, 87(1-5):1–47, jul 2008.
- [43] O. C. Zienkiewicz and R. L. Taylor. *The Finite Element Method: The basis*. Referex Engineering. Butterworth-Heinemann, 2000.

- [44] G. H. Yoon. Structural topology optimization for frequency response problem using model reduction schemes. *Computer Methods in Applied Mechanics and Engineering*, 199(25–28):1744–1763, 2010.
- [45] A. Chatterjee. An introduction to the proper orthogonal decomposition.
- [46] K. K. Choi and N. H. Kim. *Structural Sensitivity Analysis and Optimization*. Mechanical Engineering Series. Springer New York, 2006.
- [47] K. Svanberg. The method of moving asymptotes - a new method for structural optimization. *International Journal for Numerical Methods in Engineering*, 24(2):359–373, feb 1987.
- [48] H. Li, Y. Ma, W. Wen, W. Wu, H. Lei, and D. Fang. In Plane Mechanical Properties of Tetra-chiral and Antitetra-chiral Hybrid Metastructures. *Journal of Applied Mechanics*, 84(8):081006, jun 2017.
- [49] I. G. Masters and K. E. Evans. Models for the elastic deformation of honeycombs. *Composite Structures*, 35(4):403–422, 1996.
- [50] L. Xia and P. Breitkopf. Design of materials using topology optimization and energy-based homogenization approach in Matlab. *Structural and Multidisciplinary Optimization*, 52(6):1229–1241, 2015.
- [51] K. Svanberg. MMA and GCMMA-two methods for nonlinear optimization. *vol*, 1:1–15, 2007.